Available online at www.sciencedirect.com
SCIENCE DIRECT®
ELSEVIER
International Journal of Multiphase Flow 30 (2004) 51–66
International Journal of Multiphase Flow
www.elsevier.com/locate/ijmulflow

Modeling a turbulent fibre suspension flowing in a planar contraction: The one-dimensional headbox

James A. Olson [a,*], Ian Frigaard [b], Candice Chan [a], Jari P. Hämäläinen [c]

[a] *The Pulp and Paper Centre, Department of Mechanical Engineering, The University of British Columbia, 2324 Main Mall, Vancouver BC, Canada V6T 1Z4*
[b] *Department of Mathematics and Department of Mechanical Engineering, The University of British Columbia, 1984 Mathematics Road, Vancouver, BC, Canada V6T 1Z2*
[c] *Metso Paper Inc., P.O. Box 587, FIN-40101 Jyväskylä, Finland*

Received 2 August 2003; received in revised form 23 October 2003

Abstract

An Eulerian model of a turbulent fibre suspension flowing through a planar contraction is proposed to predict the fibre orientation distribution. The model specifically applies to the flow of pulp suspensions through a papermachine headbox. The model accounts for the convection of orientation distribution of the mean fluid velocity and the dispersion caused by the turbulent velocity fluctuations and describes each by a dimensionless dispersion coefficient and a dimensionless velocity gradient characterized by the contraction ratio (ratio of duct inlet height to outlet height) of the duct. A numerical solution of the model equations was shown to compare well to two different experimental studies available in the literature. From comparison with experiment the rotational dispersion coefficient was estimated to be 2 s^{-1} for both studies. Using the experimental value of the rotational dispersion coefficient and assuming it remains constant, the fibre orientation distributions was calculated for a range of dimensionless dispersion coefficients and contraction ratios. It was demonstrated that increasing the contraction ratio, over the industrial range of 5–50, significantly increases the alignment of fibres exiting the headbox. It was also shown that varying the inlet fluid velocity, over a practical range, provides only small changes in the fibre orientation distribution. Both predicted effects agree with experimental observation. Furthermore, this study suggests that fibre orientation is approximately dependent on a single dimensionless Peclet number that is a function of the fluid contraction ratio, inlet velocity, contraction length and rotational dispersion coefficient and that this parameter can be used to guide the design and operation of commercial headboxes.

* Corresponding author. Tel.: +1-604-822-5705; fax: +1-604-822-2403.
E-mail address: olson@mech.ubc.ca (J.A. Olson).

0301-9322/$ - see front matter © 2003 Elsevier Ltd. All rights reserved.
doi:10.1016/j.ijmultiphaseflow.2003.10.006

1. Introduction

Turbulent fibre suspensions are of interest in many industrial processes. They are of particular interest in the pulp and paper industry where paper is formed from dilute suspensions of cellulose fibres. During the paper forming process, at the start of the paper machine, a dilute fibre suspension flows through a specially shaped duct called a headbox. The first section of the headbox consists of a manifold that sets up a uniform flow across the 10 m wide duct. The fluid then passes through flow distributors and turbulence generators designed to produce nearly isotropic turbulence. The uniform turbulent flow subsequently passes through a planar contraction that accelerates the fluid to a high speed and creates a thin planar jet. The jet can be approximately 10 m wide, 1 cm thick with a mean velocity of more than 25 m/s. The jet then passes through two fast moving meshes that drain the water while retaining the fibres. The remaining water is subsequently evaporated to produce dry paper.

During passage through the headbox, fibres are aligned by the accelerating flow in the contraction. The degree of fibre alignment significantly affects the strength properties of the paper. Fibre alignment can be both beneficial and problematic depending on the application. For example, in high-speed printing, the paper requires high tensile strength only in the direction of travel through the printing press. Therefore, high fibre alignment is preferable. Whereas, in paper sack production the paper is required to be equally strong in all directions, thus uniform fibre orientation is preferred. The effect of fibre orientation on paper properties, both in the plane of the paper and in the paper thickness direction is reviewed by Loewen (1997).

To better understand the effect of headbox design and operation on fibre orientation, several fundamental studies have experimentally examined the orientation distribution of fibres in suspension as they pass through a transparent laboratory headbox. In studies by Ullmar (1998) and Ullmar and Norman (1997), the fibre orientation distribution in the plane of the paper was measured at the headbox exit by electronically imaging nylon fibres in suspension. These studies examined the effect of mean flow through the headbox, contraction ratio and fibre concentration. In a more recent study conducted by Zhang (2001), the fiber orientation distribution was measured in both the plane of the paper and in the plane of the contraction at several locations along the axis of the headbox. Fibre orientation distributions were measured for a range of inlet flow rates. In the studies by Zhang (2001) and Olson (2001b) it was shown that if turbulent dispersion is neglected the theoretically predicted fibre orientation distribution significantly over predicts the degree of fibre alignment when compared with that observed experimentally. Therefore, it was concluded that predicting fibre orientation in headbox flow requires the effects of fluid turbulence to be considered.

In this study, a theoretical model of the orientation distribution of fibres moving in a turbulent planar contraction is developed and the predictions are compared with experimental measurements in the literature. The model is then used to explore the effects of headbox design and operation.

2. Background

There are two methods to model turbulent particle suspensions, the Lagrangian approach and the Eulerian approach. In the Lagrangian approach, the trajectory of a single particle is

calculated by solving the particles equations of motion through a known mean and fluctuating flow field. For spherical particles, this method has been used by many investigators (for example Lu et al., 1993; MacInnes and Bracco, 1992; Call and Kennedy, 1992). In addition, several investigators have used Lagrangian methods to estimate the fibre orientation and concentration distribution in various flows regimes. These include Riese et al. (1969), Shanker et al. (1991), Pittman and Kasiri (1992), Tangsaghasaksri (1994), Olson (1996) and Olson (2001a,b). Furthermore, this method has been used by Zhang (2001) to model fibre orientation in headbox flows of interest to this study. In the Eulerian approach, the probability distribution of fibre orientation and position is calculated using a convection–dispersion equation or Fokker–Plank equation. In this approach, the mean flow convects the fibres position and orientation distribution and the fluctuating component of the flow disperses fibres creating a flux opposite to the gradient of the fibre position and orientation distribution. For spherical particles this method has been used by many investigators to calculate particle concentration, including Hinze (1975), Hishida et al. (1992). The Eulerian approach has several advantages for modeling turbulent fibre suspensions. It is computationally more efficient and has the potential to account for the complex fibre–fibre interactions and the modification of the fluid turbulence by the presence of the fibres. The Eulerian approach has been used extensively in the field of polymer rheology to calculate the orientation and concentration of linear polymer molecules in suspension (see for example Doi and Edwards, 1988). In this application, the Brownian motion of the surrounding polymeric molecules causes rotational and translational dispersion. This is analogous to turbulent flow where the turbulent fluctuations lead to dispersion.

For both applications, the Eulerian convection–dispersion equation that describes the change of fibre orientation, $\boldsymbol{p}$, and position, $\boldsymbol{r}$, probability distribution, $\Psi(\boldsymbol{r},\boldsymbol{p},t)$, is given by

$$\frac{\partial \Psi}{\partial t} = D_{\mathrm{p}}\nabla_{\mathrm{r}}^2\Psi - \nabla_{\mathrm{r}}\cdot(\boldsymbol{\omega}\Psi) + D_{\mathrm{t}}\nabla^2\Psi - \nabla\cdot(\overline{\boldsymbol{V}}\Psi), \tag{1}$$

where D_{t} is the translational dispersion coefficient, $\overline{V}$ is the mean translational velocity, D_{p} is the angular dispersion coefficient and ∇_{r} is sometimes referred to as the rotational operator, and is expressed as

$$\nabla_{\mathrm{r}} = \boldsymbol{p}\times\frac{\partial}{\partial \boldsymbol{p}}. \tag{2}$$

The fibre's angular velocity, $\boldsymbol{\omega}$, is related to the fibres rotational vector by the following,

$$\boldsymbol{\omega} = \boldsymbol{p}\times\dot{\boldsymbol{p}}. \tag{3}$$

In applications to turbulent flow, the difficulty lies in relating the rotational and translational dispersion coefficients to the properties of the fluid turbulence.

The orientation distribution function of small fibres in turbulent flow has also been theoretically calculated by Krushkal and Gallily (1988) using Eq. (1). The dispersion coefficient was assumed to be influenced by the local turbulence of the flow and a relationship based on Kolmogoroff's local isotropy hypothesis for the very small eddies of the turbulence spectrum was used. From this assumption, the rotational dispersion coefficient was related to the turbulent dissipation, ϵ, and the kinematic viscosity, v, by dimensional analysis as $D_{\mathrm{p}} = (\epsilon/v)^{1/2}$ which was related to the fluctuating component of the fluids velocity, u_i, by $\epsilon/v = \sum_{ij}\overline{\left(\frac{\mathrm{d}u_i}{\mathrm{d}\xi_j}\right)^2}$.

More recently, Olson and Kerekes (1998) developed an analytic estimate of the rotational and translational turbulent dispersion coefficients by considering a statistical analysis of the equations of motion for a single fibre moving in homogeneous, isotropic turbulence. Their analysis relates the rotational dispersion coefficient to the fluid's velocity correlation as,

$$D_{\mathrm{p}} = \frac{1}{2}\frac{\mathrm{d}}{\mathrm{d}t}\left(\overline{u^2}\frac{24}{L^3}\int_0^t\int_0^{L_{\mathrm{f}}} 2(t-\tau)\left(1-3\frac{\delta}{L}+2\left(\frac{\delta}{L}\right)^3\right)R_v(\delta,\tau)\,\mathrm{d}\delta\,\mathrm{d}\tau\right) \tag{4}$$

where $R_v(\delta,\tau)$ is approximately equal to the velocity correlation of the fluid. In the limit as fibre length, L_{f}, becomes smaller than the integral length scale of the turbulence, the long time orientation dispersion coefficient becomes

$$D_{\mathrm{p}} = 2\frac{\overline{u^2}}{\lambda^2}T \tag{5}$$

where λ is the Taylor micro-length scale, or dissipation scale of the turbulence, which represents the average dimension of the smallest eddies (Hinze, 1975) and T is the Lagrangian integral time scale of the fluid. In further work, Olson (2001a,b) demonstrated that the orientation dispersion coefficient could be estimated from the kinetic energy and dissipation rate, commonly used in turbulence modeling, as

$$D_{\mathrm{p}} \approx 0.7\left(\frac{4\epsilon}{15\nu}\right)^{1/2} \tag{6}$$

which is similar to that given by dimensional analysis of Krushkal and Gallily. Unfortunately, it has been shown that κ–ϵ models of the flow in planar contractions does not accurately predict the length scales of the turbulence (Parsheh, 2001) and, therefore, may not provide a good estimate of the dispersion coefficient.

Estimating the rotational dispersion coefficient relies on estimating the Lagrangian integral time scale, the dissipation length scale and the magnitude of the velocity fluctuations. Parsheh (2001), experimentally measured the turbulent characteristics of grid generated turbulent flow that subsequently passes through a planar contraction. Parsheh showed that the velocity fluctuations perpendicular to the flow direction are approximately equivalent and increased slightly during the contraction. The streamwise fluctuations remained approximately constant with a small minimum shortly after the headbox inlet. Parsheh compared his result to those predicted by rapid distortion theory (RDT) and to computations using Reynolds average Navier–Stokes (RANS) turbulence modeling methods. From this comparison, it was determined that the experimental measurements differed considerably from that predicted by RDT. The computational predictions showed similar trends to the experimental measurements, but that the computational results were strongly dependent on the dissipation length scale assumed in the flow. Parsheh showed that the best correlation between the computational predictions and the experimental measurements occurred when the dissipation length scale was assumed to be constant along the length of the contraction. This implies that the rotational dispersion may be best modeled by assuming a constant dispersion coefficient through the contraction.

Clearly, the lack of available computational estimates or experimental measurements of dissipation length-scale makes it difficult to predict the magnitude of the rotational dispersion coefficient necessary to model the fibre orientation distribution changes in the headbox. Therefore, in this study, the rotational dispersion coefficient is assumed to be constant along the central streamline of the contraction. Using this assumption, the magnitude of the rotational dispersion coefficient can now be estimated by comparing experimental measurements of fibre orientation, available in the literature, with the fibre orientation predicted using a simplified form of Eq. (1). Furthermore, the estimated dispersion coefficient is used in conjunction with the simplified form of Eq. (1), referred to as the one-dimensional headbox model, to determine the effects of the headbox design and operation variables on fibre orientation.

3. The one dimensional headbox

A simplified model of the orientation distribution of fibres moving through the headbox is derived by first considering the equations of motion for a straight rigid inertialess fibre moving along the central streamline of the planar contraction. From the equation of mean rotation, the simplified form of Eq. (1) is derived for fibre orientation in the plane of the free jet and in the plane of the contraction. The equations of mean rotation for fibres in a dilute, turbulent flow have been derived previously by Olson and Kerekes (1998) in terms of the average flow field $\boldsymbol{u}$, assuming a straight, rigid, infinitely thin, inertialess fibre acted on by a constant drag tensor (Cox (1970)).

The equation of mean translation $\boldsymbol{v}$, is given by

$$\boldsymbol{v} = \frac{1}{L_f} \int_{-L_f/2}^{L_f/2} \boldsymbol{u}(\boldsymbol{y} + l\boldsymbol{p}, t)\mathrm{d}l \tag{7}$$

where $\boldsymbol{y}$ is the position, $\boldsymbol{p}$ a unit vector in the direction of the fibre and l is the distance along the fibre from the centre (see Fig. 1). The mean rotation is given by

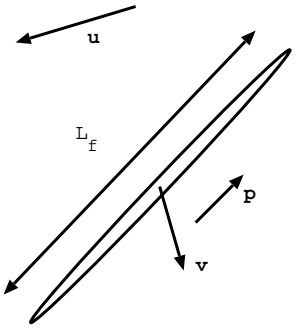

Fig. 1. A straight rigid fibre of length L_f, moving with velocity $\boldsymbol{v}$, in a turbulent fluid with velocity $\boldsymbol{u}$. The fibre is pointing in the direction given by unit vector $\boldsymbol{p}$.

$$\boldsymbol{\Omega} = \boldsymbol{p} \times \frac{12}{L_f^3} \int_{-L_f/2}^{L_f/2} l\boldsymbol{u}(\boldsymbol{y} + l\boldsymbol{p}, t)\mathrm{d}l \tag{8}$$

where Ω is the angular velocity of the fibre. The rate of change of orientation, $\dot{\boldsymbol{p}}$, is then calculated as

$$\dot{\boldsymbol{p}} = \boldsymbol{\Omega} \times \boldsymbol{p} \tag{9}$$

These equations for fibre motion have been used to model a fibre moving in non-homogeneous flows, e.g., non-linear shear, by several investigators (Riese et al., 1969; Shanker et al., 1991; Pittman and Kasiri, 1992; Tangsaghasaksri, 1994; Olson, 1996).

For a linear velocity gradient, the angular velocity of the fibres projection in the x–y plane (see Fig. 2), $\dot{\phi}$, is given in terms of its component partial derivatives for planar flow where $\boldsymbol{u} = \boldsymbol{u}(u(x,y), v(x,y))$, that is,

$$\dot{\phi} = \frac{1}{2}\left(\frac{\partial v}{\partial y} - \frac{\partial u}{\partial x}\right)\sin(2\phi) - \frac{\partial u}{\partial y}\sin^2(\phi) + \frac{\partial v}{\partial x}\cos^2(\phi) \tag{10}$$

This equation is general for a fibre rotating in a linear flow field and is identical to that of Jeffery (1922) in the limit of large fibre aspect ratio. It is also interesting to point out that $\dot{\phi}$ is independent of the angle θ. This fact greatly simplifies the calculation of orientation distribution of ϕ.

To calculate the mean translational and rotational velocity of the fibre, the mean flow field in the planar contraction needs to be defined. The mean flow in a planar symmetric contraction is assumed to be approximately one-dimensional, especially along the central streamline, $y = 0$, where we apply this analysis. We assume a linear taper and define the walls, $y = \pm y_h$, of the headbox by the following shape Fig. 3

$$y_h = y_s + y_0 - y_0\left(\frac{x}{L}\right) \tag{11}$$

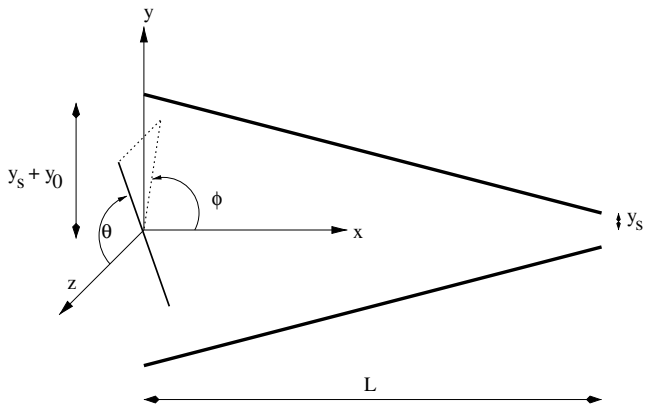

Fig. 2. The orientation of a fibre with respect to the flow in the headbox. The angle ϕ is the angle of the projection of the fibre in the xy-plane (plane of the contraction).

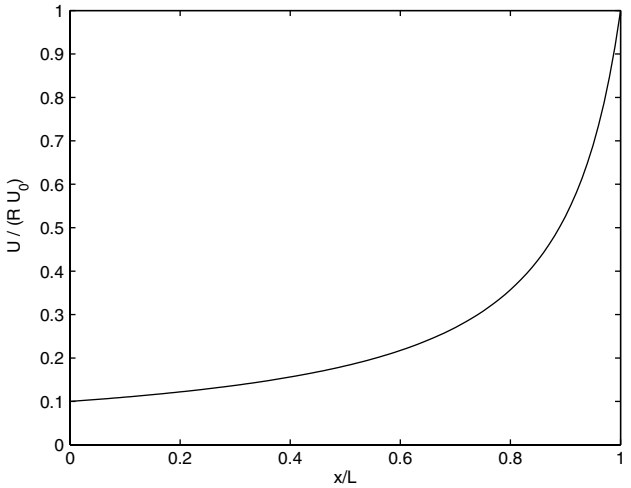

Fig. 3. The fluid velocity, u, as a function of distance through the headbox, $R = 10$.

where $y_0 + y_s$ is the initial half height of the headbox, y_s is the final half height of the slice, x is the position along the length of the headbox and L is the length of the headbox. For an incompressible, one-dimensional flow continuity implies

$$u(x)2y_h = \text{const.} \tag{12}$$

that is,

$$u(x) = \frac{u(0)}{1 - \left(1 - \frac{1}{R}\right)\left(\frac{x}{L}\right)} \tag{13}$$

where $R = \frac{y_0 + y_s}{y_s}$ is the contraction ratio of the headbox. The fluid velocity as a function of distance x/L through the headbox is given in Fig. 4. This estimate of the velocity distribution along the central streamline compares well to the experimental measurements of Parsheh (2001) and with that computed by Zhang (2001) using a $k - \epsilon$, CFD simulation.

The one dimensional headbox problem considers only the mean translation of the fibres along the central streamline. Translational dispersion, both in the direction of the flow and perpendicular to the flow direction, are neglected. Furthermore, the model only considers the distribution of the projected angle of the fibre, ϕ which is independent of the azimuthal angle θ. From these assumptions Eq. (1) can be simplified to

$$\frac{\partial \Psi}{\partial t} + u\frac{\partial \Psi}{\partial x} = D_p \frac{\partial^2 \Psi}{\partial \phi^2} - \frac{\partial(\dot{\phi}\Psi)}{\partial \phi} \tag{14}$$

Eq. (14) is further simplified by assuming steady flow, and made dimensionless by scaling variables by headbox length, L, and inlet velocity u_0 such that $\bar{x} = \frac{x}{L}$ and $\bar{u} = \frac{u}{u_0}$. This results in the following dimensionless form of Eq. (14),

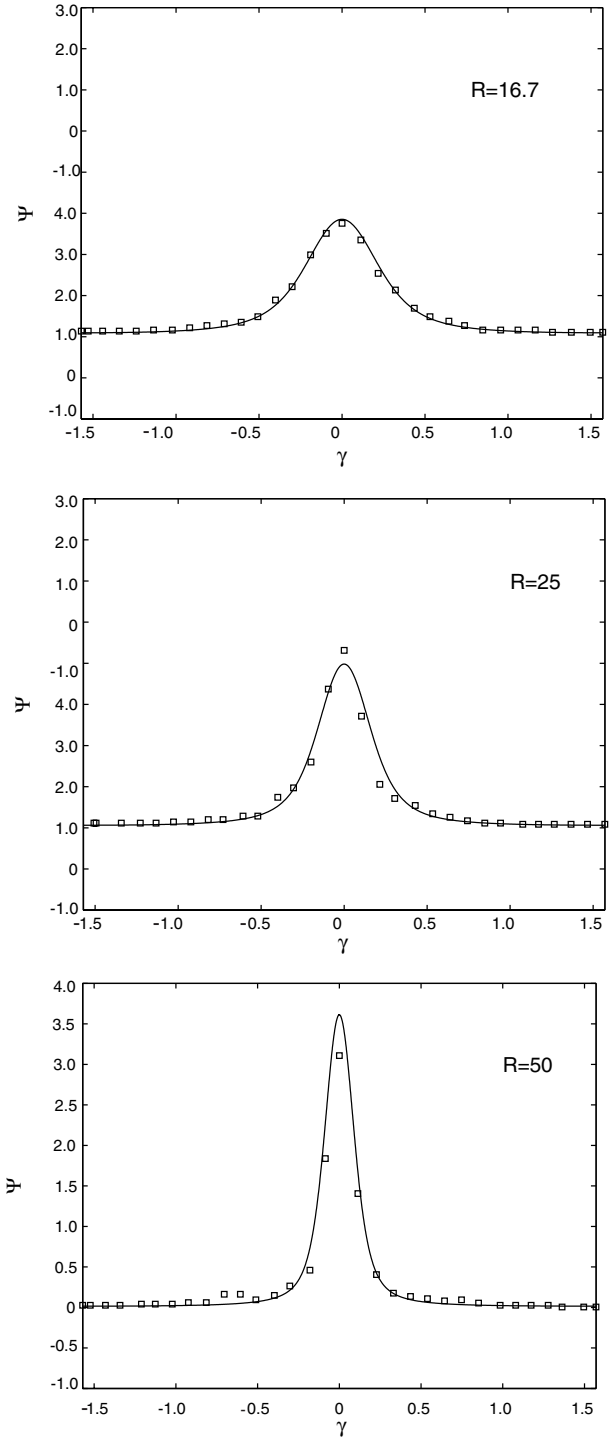

Fig. 4. Comparison of computed orientation distribution, Ψ, to the experimental measurements of Ullmar (1998) for three contraction ratios of $R = 16.7$, 25 and 50.

$$\bar{u}\frac{\partial \Psi}{\partial \bar{x}} = \overline{D}_{\mathrm{p}}\frac{\partial^2 \Psi}{\partial \phi^2} - \frac{\partial(\dot{\phi}\Psi)}{\partial \phi} \tag{15}$$

where $\overline{D}_{\mathrm{p}} = \frac{LD_{\mathrm{p}}}{u_0}$ is the dimensionless dispersion coefficient and the mean angular velocity of the fibre, $\dot{\phi}$, is given by

$$\dot{\phi} = -\frac{\partial \bar{u}}{\partial \bar{x}}\sin(2\phi) \tag{16}$$

Substituting Eq. (16) into Eq. (15) results in the following expression for fibre orientation in the plane of the contraction.

$$\bar{u}\frac{\partial \Psi}{\partial \bar{x}} = \overline{D}_{\mathrm{p}}\frac{\partial^2 \Psi}{\partial \phi^2} + \frac{\partial \bar{u}}{\partial \bar{x}}\frac{\partial(\sin(2\phi)\Psi)}{\partial \phi} \tag{17}$$

where the initial fibre orientation is assumed to be uniformly distributed, i.e., Eq. (17) has the boundary condition $\Psi(x = 0) = \pi^{-1}$.

Eq. (17) is the same form as the standard convection–diffusion equation used to model molecular diffusion or heat transfer. However, in this application the convection is in fibre orientation angle as opposed to fibre position, the orientational diffusion is due to turbulent dispersion and evolution is with respect to x as opposed to time. The ratio of convection to dispersion along the length of the contraction is defined as the local Peclet number, Pe_{l}, and is given by

$$Pe_{\mathrm{l}} = \frac{\frac{\partial \bar{u}}{\partial \bar{x}}}{\overline{D}_{\mathrm{p}}} \tag{18}$$

Along the contraction, Pe_{l} varies non-linearly, increasing significantly near the exit of the contraction where the acceleration of the flow is highest.

The Peclet number for the entire headbox flow is estimated by linearizing the fluid velocity and noting that

$$\frac{\partial \bar{u}}{\partial \bar{x}} \approx R \tag{19}$$

Thus the average Peclet number for the headbox is

$$Pe = \frac{R}{D_{\mathrm{p}}} = \frac{u_0 R}{L\overline{D}_{\mathrm{p}}} \tag{20}$$

which combines the importance design and operating variables of the headbox.

The fibre orientation distribution in the plane of the paper, γ is similarly calculated by substituting γ for ϕ, knowing that

$$\dot{\gamma} = -\frac{1}{2}\frac{\partial \bar{u}}{\partial \bar{x}}\sin(2\gamma). \tag{21}$$

It is interesting to point out that the mean rotational velocity in the plane of the contraction is half the magnitude of the rotational velocity in the plane of the jet.

The resulting fibre orientation distribution at the headbox exit, $\Psi(\phi)$ or $\Psi(\gamma)$, is a function of the dimensionless dispersion coefficient $\overline{D}_p$ and the contraction ratio R of the headbox. Although, the Peclet number does not account for the non-linearity of the local Peclet number, it is still expected that headbox flows with similar Peclet numbers will have similar fibre orientation distribution.

4. Results and discussion

4.1. Solution method

The fibre orientation distribution is determined by solving Eq. (17) numerically. This has been done using both finite difference and finite element methods as described in Brooks and Hughes (1982) and Skeel and Berzins (1990). The solution for both methods were shown to be the same for the range of $\overline{D}_p$ and R computed below. We use the implicit Euler and Crack–Nicolson methods for the x-derivative. When the x-derivative is considered as time, Eq. (17) has only one spatial co-ordinate, the fibre orientation. The other terms of Eq. (17) are discretized by using the Streamline Upwind/Petrov–Galerkin method (SUPG) (Brooks and Hughes, 1982) which has been developed for convection-dominated problems. It is also important to use a locally refined finite element mesh near $\phi = 0$ in order to capture very high gradients of fibre orientation angle. At the headbox inlet to the contraction, we assume that fibres are randomly distributed, i.e., $\Psi = 1/\pi$, and we use this one as a Dirichlet boundary condition. It agrees well with the experimental measurements in the literature (Ullmar, 1998; Zhang, 2001). For the angles $\phi = -\pi/2$ and $+\pi/2$ we impose homogeneous Neumann boundary conditions.

4.2. Comparison with experiments in the literature

The computed fibre orientation distributions are compared with the experimental measurements of Ullmar (1998) and Ullmar and Norman (1997). In these experiments, fibre orientation was determined for nylon fibres flowing in a dilute suspension through a transparent headbox. The fibre orientation was determined by imaging the fibres in the plane of the jet, at the exit of the headbox and measuring the angle between axis of the fibre and the central streamline.

Fig. 4 shows the experimental fibre orientation distributions measured for three contraction ratios ($R = 16.7$, 25, 50) compared to that calculated from Eq. (15) for a best fit value of $D_p = 2$ s^{-1}. Fig. 4 demonstrates the strong agreement between the computed and experimental fibre orientation distributions. Fig. 4 also shows the strong effect of contraction ratio on the degree of fibre alignment. Increased contraction ratio results in significantly higher fibre alignment in the direction of flow. The magnitude of the dimensionless dispersion coefficient, $\overline{D}_p = 2.5$, corresponds to Peclet number's equal to 6.7, 10 and 20 for contraction ratios of 16.7, 25 and 50, respectively. This indicates that the magnitude of the turbulent dispersion is approximately an order of magnitude less than the convection from the mean flow, except when the concentration

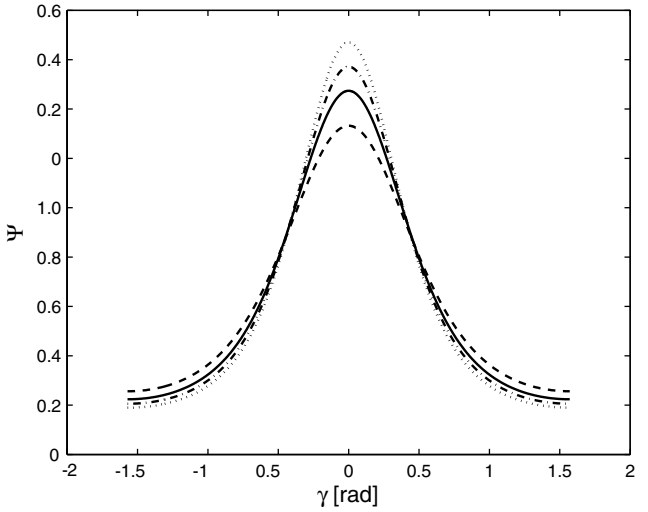

Fig. 5. Theoretical fibre orientation distribution for varying $\overline{D}_p$ corresponding to $u(0) = 0.2$ (dashed), 0.27 (solid line), 0.33 (dash dot line) and 0.4 m/s (dotted line) at a contraction ratio, $R = 25$, corresponding to the experiments of Ullmar (1998).

gradient is very high. Furthermore, the rotational dispersion coefficient is assumed to be constant and equal to $D_p = 2\ s^{-1}$ for all three contraction ratio's.

Ullmar also conducted experiments where the fluid velocity of the jet exiting the duct varied between 5 and 10.0 m/s and saw only a small change in fibre orientation. Fig. 5 shows the computed theoretical fibre orientation distributions for the same range of flow velocities assuming a constant rotational dispersion coefficient. Figure indicates that fibre orientation is weakly dependent on inlet flow velocity in agreement with the experimental observations.

In a more recent study conducted by Zhang (2001), the fiber orientation distribution was measured in both the plane of the paper and in the plane of the contraction at several locations along the axis of the headbox. The contraction ratio of the headbox was equal to 10. Fig. 6 compares the experimental fibre orientation distributions and the theoretical fibre orientation distributions for the same value of dispersion coefficient, $D_p = 2\ s^{-1}$ as used in the comparison with Ullmar. Fig. 6 demonstrates a good correlation for both γ and ϕ throughout the headbox. Both the experimental and theoretical fibre orientation distributions indicate that fibres are significantly more aligned in the the plane of the contraction, i.e., $\Psi(\phi)$, than they are aligned in the plane of the paper, i.e., $\Psi(\gamma)$. From theory, the increased alignment in the plane of the contraction is due to the increased mean rotational velocity as predicted by Eqs. (16) and (21). Furthermore, Fig. 6 shows that most of the alignment occurs near the end of the headbox, beyond $x/L = 0.75$, where the velocity gradient thus the orientational velocity is the highest. This effect is also predicted by the model. The good correlation between the model and experiment indicates that the model provides a good estimate of the mean rotational velocity of the fibres.

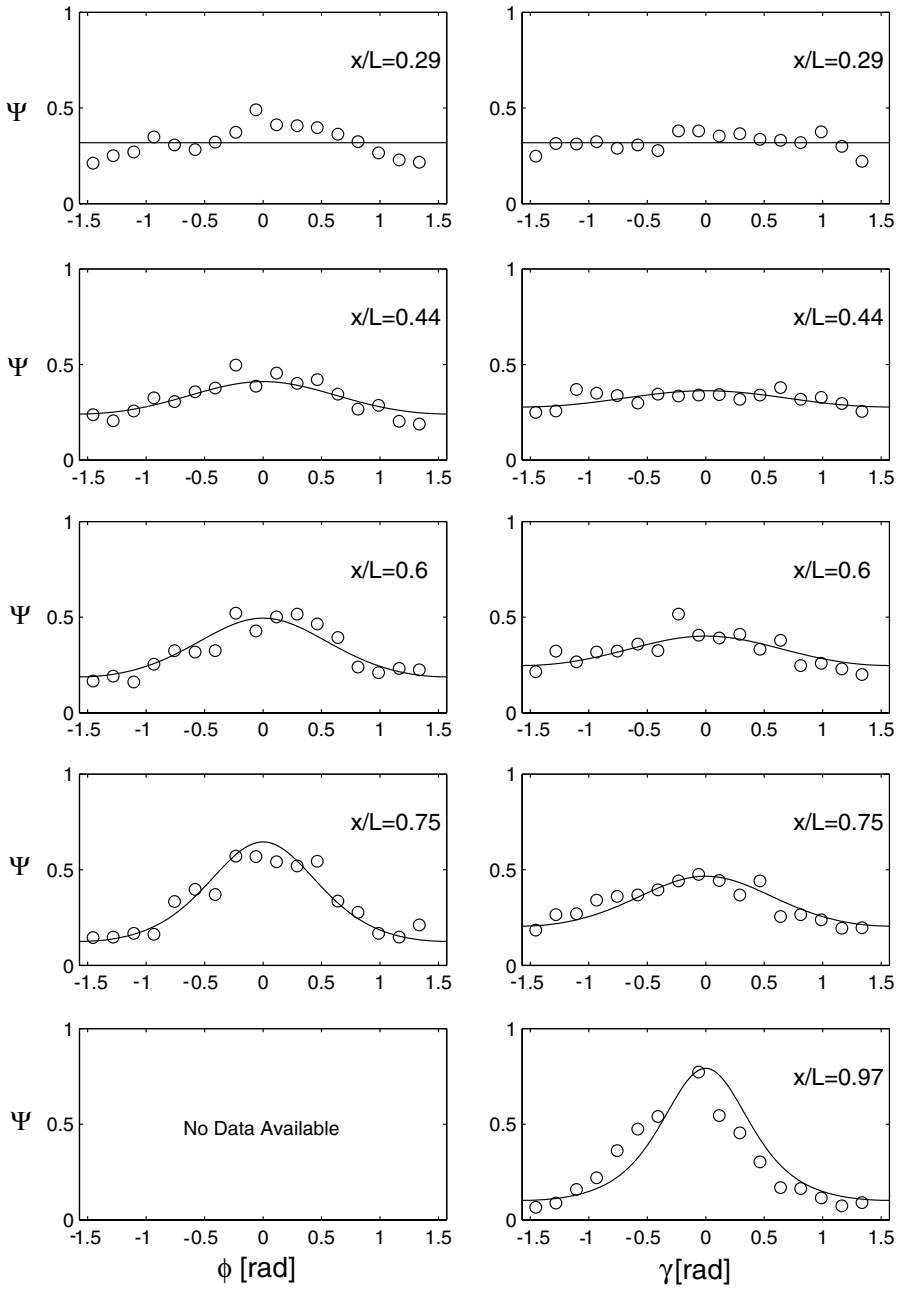

Fig. 6. Comparison of theoretical Ψ for both γ and ϕ to the experimental measurements made by Zhang (2001) as a function of position through the headbox, x/L. Note that no measurements of ϕ were made at $x/L = 0.97$.

The fact that the same value of the rotational dispersion coefficient provided a good fit to the data obtained in both experimental studies suggests that the turbulent properties of both flows are

similar. This is probably because the size of the two apparatus were similar and both used a turbulence generating section of similar scale to setup the nearly isotropic turbulence at the inlet of the duct. In the general case, it is expected that the rotational dispersion coefficient will change as the scale of the turbulence changes. However, for industrial headboxes with similar turbulence generating components, the results should extend to predict their performance.

4.3. Effect of $\overline{D}_p$ and R

To demonstrate the effect of varying the rotational dispersion coefficient $\overline{D}_\mathrm{p}$ on the fibre orientation in the plane of the jet, Eq. (15) was solved for $R = 25$ and $\overline{D}_\mathrm{p} = 0.01$, 0.1, 1.0, 2.5, 10, and 100, and are plotted in Fig. 7. For very small dispersion, $\overline{D}_\mathrm{p} \approx 0$, the numerical solution was equivalent to the analytic solution given by Olson (2001b),

$$\Psi(\gamma) = \frac{(1 + \tan^2(\gamma))R}{1 + R^2 \tan^2(\gamma)}\pi^{-1} \tag{22}$$

Fig. 7 shows that for small values of the dimensionless dispersion coefficient the fibres are strongly aligned in the direction of flow and that for larger values of the dimensionless dispersion coefficient fibre orientation is significantly more random.

Similarly, Fig. 8 shows the effect of increasing contraction ratio from 5 to 50 for a constant $\overline{D}_\mathrm{p} = 2.5$. The figure demonstrates how increasing contraction ratio can have a significant effect on fibre alignment. For small values of contraction ratio the fibres are only weakly aligned in the direction of flow, while larger values of contraction ratio strongly align the fibres.

Previously, it was proposed that the Peclet number describing fibre orientation in a planar contraction could be approximated as $Pe = R/\overline{D}_\mathrm{p}$ and that similar Pe values would result in similar

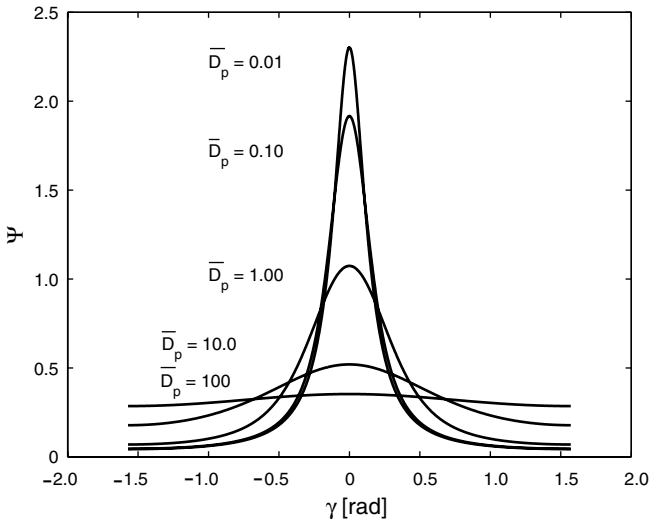

Fig. 7. Theoretical fibre orientation distribution for varying $\overline{D}_\mathrm{p}$ for constant contraction ratio, $R = 25$, at the headbox exit ($x = L$).

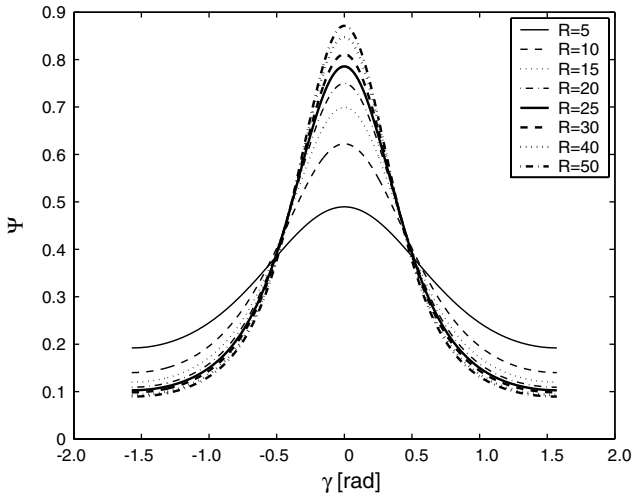

Fig. 8. Theoretical fibre orientation for varying contraction ratio and constant $D_p = 2\ s^{-1}$, at the headbox exit ($x = L$).

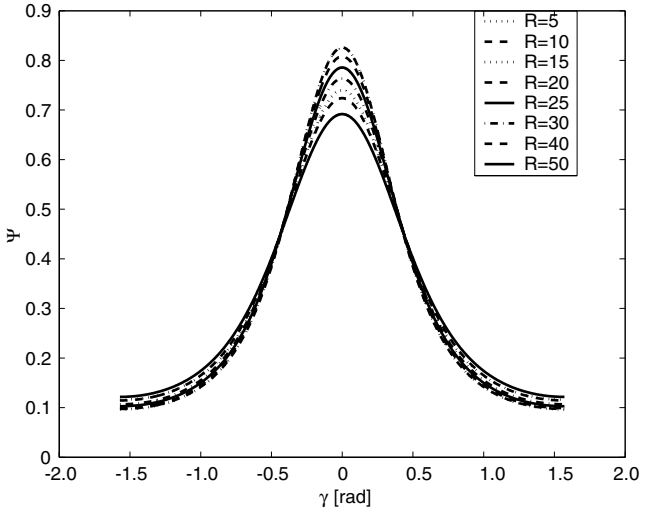

Fig. 9. Theoretical fibre orientation for constant Peclet number, $Pe = 10$, at the headbox exit ($x = L$).

fibre orientation distributions. To demonstrate this, Fig. 9 shows the fibre orientation distribution for a range of contraction ratios, from $R = 5$ to 50, but all with $Pe = 10$. From Fig. 9, it is evident that for the same Peclet number the fibre orientation distributions are approximately equivalent. The difference between distributions are due to the non-linearity of the local Peclet number along the central streamline, that is, fibres align more rapidly at the end of the headbox where the fluids acceleration is the highest and this effect increases as contraction ratio increases.

5. Conclusions

In this study, the one-dimensional headbox model is derived to predict the orientation distribution of fibres in a turbulent suspension passing through a planar contraction. The proposed one-dimensional headbox model was solved numerically and shown to accurately predict the experimentally observed fibre orientation distribution for a wide range of contraction ratios and inlet velocities.

From the model it is determined that the fibre orientation distribution is a function of two non-dimensional parameters, the dimensionless dispersion coefficient and the headbox contraction ratio. The dimensionless dispersion coefficient is the a function of the headbox length, inlet flow velocity and the rotational dispersion coefficient and indicates the magnitude of the turbulent dispersion. The contraction ratio approximates the average dimensionless acceleration of the fluid and indicates the magnitude of the convection. Contraction ratio was shown to strongly affect fibre alignment and that contraction ratios to greater than 25 results a high degree of fibre alignment at the headbox exit. Comparison with experimental measurements shows that the rotational dispersion coefficient is approximately equal to 2 s^{-1}, and that for typical headboxes the Peclet number will range from 2 to 20 indicating that the magnitude of the turbulent dispersion is of the same order as the convection from the mean flow. Furthermore, it was shown that fibre orientation distribution was approximately dependent on the headbox Peclet number, defined as the ratio of contraction ratio to dimensionless dispersion coefficient.

Acknowledgements

J.A. Olson would like to acknowledge support from the Natural Sciences and Engineering Research Council of Canada (NSERRC) and by the Univeristy of British Columbia Advanced Papermaking Initiative. I. Frigaard would like to acknowledge support from the British Columbia Advanced Systems Institute and NSERC. J.P. Hämäläinen would like to thank Dr. Kai Hiltunen from Numerola Oy.

References

Brooks, A.N., Hughes, T.J.R., 1982. Streamline upwind/Petrov–Galerkin formulations for convection dominated flows with particular emphasis on the incompressible Navier–Stokes equations. Comput. Meth. Appl. Mech. Eng. 32, 199–259.

Call, C.J., Kennedy, J.M., 1992. Measurements and simulations of particle dispersion in a turbulent flow. Int. J. Multiphase Flow 18, 891–903.

Cox, R.G., 1970. The motion of long slender bodies in a viscous fluid. part 1. general theory. J. Fluid Mech. 44, 791–810.

Doi, M., Edwards, S.F., 1988. The Theory of Polymer Dynamics. Clarendon Press, Oxford.

Hinze, J.O., 1975. Turbulence, second ed. McGraw-Hill Inc., New York.

Hishida, K., Ando, A., Maieda, M., 1992. Experiments on particle dispersion in a turbulent mixing layer. Int. J. Multiphase Flow 18, 181–194.

Jeffery, G.B., 1922. The motion of ellipsoidal particles immersed in a viscous fluid. Proc. Royal Soc. A 102, 161–179.

Krushkal, E.M., Gallily, I., 1988. On the orientation distribution function of non-spherical aerosol particles in a general shear flow—ii. the turbulent case. J. Aerosol Sci. 19, 197–211.

Loewen, S.R., 1997. Fibre orientation optimization. Pulp and Paper Canada 19, 25–27.

Lu, Q., Fontaine, J.R., Aubertin, G., 1993. Langrangian model for solid particles in turbulent flows. Int. J. Multiphase Flow 19, 347–367.

MacInnes, J.M., Bracco, F.V., 1992. Stochastic particle modelling and the tracer-particle limit. Phys. Fluids A 4, 2809–2824.

Olson, J.A., 1996. The effect of fibre length on passage through narrow apertures. PhD thesis, The University of British Columbia, Vancouver.

Olson, J.A., Kerekes, R.J., 1998. The motion of fibres in turbulent flow. J. Fluid Mech. 377, 47–64.

Olson, J.A., 2001a. Analytic estimate of fibre orientation in a headbox flow. Nordic Pulp Paper Res. J. 17, 302–306.

Olson, J.A., 2001b. The motion of fibres in turbulent flow, stochastic simulation of isotropic homogeneous turbulence. Int. J. Multiphase Flow 27, 2083–2103.

Parsheh, M., 2001. Flow in contractions with application to headboxes. PhD thesis, Royal Institute of Technology, Sweden.

Pittman, J.F.T., Kasiri, N., 1992. The motion of rigid rod-like particles suspended in non-homogeneous flow fields. Int. J. Multiphase Flow 18, 1077–1091.

Riese, J., Spiegelberg, H., Ebeling, K., 1969. Mechanism of screening: dilute suspensions of stiff fibres at normal incidence. Tappi J. 52, 895–903.

Shanker, R., Gillespie Jr., J.W., Guceri, S.I., 1991. On the effect of nonhomogeneous flow fields on the orientation distribution and rheology of fibre suspensions. Polym. Eng. Sci. 31, 161–171.

Skeel, R.D., Berzins, M., 1990. A method for the spatial discretization of parabolic equations in one space variable. SIAM J. Scient. Stat. Comput. 11, 1–32.

Tangsaghasaksri, W., 1994. Über die Sortierung von Fasersuspensionen mittels geschlitzter Siebe. PhD thesis, Darmstad.

Ullmar, M., Norman, B., 1997. Observation of fibre orientation in a headbox nozzle at low consistency. In: TAPPI Proceedings, Engineering and Papermakers Conference, Anaheim, pp. 865–869.

Ullmar, M., 1998. On fibre orientation mechanisms in a headbox nozzle. Master's thesis, Royal Insititute of Technology, Stockholm.

Zhang, X., 2001. Fibre orientation in a headbox. Master's thesis, Mechanical Engineering Department, The University of British Columbia.